ADVANCED OPTICAL MATERIALS
www.advopticalmat.de

Electrically Switchable Color Tags Based on Active Liquid-Crystal Plasmonic Metasurface Platform

Mukesh Sharma, Netta Hendler, and Tal Ellenbogen*

Recent demonstrations of metasurfaces show their great potential to realize flat and multifunctional optical elements, viable for many new device applications. Yet, a major frontier in this field is to develop active, tunable, and reconfigurable metasurface platforms. These are highly desirable in modern technologies that require dynamic modulation of light. To achieve this goal, in this work an active liquid-crystal (LC) plasmonic metasurface integrated system is developed and studied. It is specifically used to demonstrate electrically switchable plasmonic-metasurface-based color tags. The active tags utilize the ability to rotate the polarization of incident light, by application of an external electric field on twisted nematic liquid crystal configuration. Combined with the wavelength and polarization-selective response of the metasurface, it allows to obtain electrically controlled transmission colors potentially spanning the entire visible spectrum. It is experimentally demonstrated that the dynamic wavelength shift in the devices is greater than 100 nm at a low driving voltage varying from 0 to 5 V. These experimental results indicate the potential of active LC-plasmonic metasurface platforms to realize the next-generation dynamic optical devices.

Active control of plasmonic metasurfaces attracts a major interest, due to its direct effect on the development of the next generation of novel dynamic optical devices, such as active color filters, high-resolution displays, imaging sensors, laser beam steering devices, optical data storage, and security devices.[1–10] In principle, plasmonic metasurface based devices usually utilize the localized surface plasmon resonance (LSPR) in metallic nanoparticles,[11] which exhibits local field enhancement, in addition to enhanced absorption and scattering of light at the resonance wavelength.[11] The LSPR wavelength is strongly dependent on the structural shape and size of the nanoparticle, the polarization of incoming light, and the surrounding dielectric medium. This was shown to provide a promising way to generate, as well as modulate, color in the visible region with high efficiency.[4,8,11–15] Therefore, plasmonic metasurfaces are attractive for use in high-resolution color displays, counterfeiting elements, and various imaging applications. However, the functionality of the metasurfaces is usually limited, due to their physical design properties, which are fixed once device is fabricated. In order to overcome this limitation, and to realize dynamically controlled devices, a mechanism for strong and tunable light–matter interaction needs to be introduced within a thin layer of active material. This has led to an extensive search for new active materials that offer highly dynamic and tunable responses.[1,5–13]

For this goal, liquid crystals (LCs) are promising active materials that exhibit large optical birefringence, ability to control the polarization of incoming light, and most importantly the LC molecules can be efficiently controlled by external electric or magnetic fields, light, and temperature.[16,17] It was shown that LCs possess the highest birefringence compared to any other natural materials over the entire visible–IR–THz–microwave spectrum, together with low power consumption and low operating voltage. Therefore, the LC based active control mechanisms have a significant advantage over other suggested mechanism to develop active metasurface platforms.[4–8,18–21]

Recently, some studies[22–32] have reported on nematic LC enabled metasurfaces that were activated by two different methods. One method was based on the ability to control the LC dielectric constants by external stimuli, which in turn can significantly influence the resonant response of the metasurface. The other approach was based on the ability to rotate the polarization of incoming light by a twisted nematic LC (TN-LC) configuration, and utilize the polarization selectivity of the metasurfaces. Specifically, for color manipulation applications, Olson et al.[22] have employed a TN-LC layer over plasmonic nanorod arrays and demonstrated that the intensity of the plasmonic color pixels can be modulated with an applied voltage. This approach can be used in order to replace the color filters in conventional Bayer pattern, where the combination of three different color pixels is required. Lee et al.[27] proposed an asymmetric lattice nanohole array based electrically tunable

Dr. M. Sharma, Prof. T. Ellenbogen
Department of Physical Electronics
Faculty of Engineering
Tel-Aviv University
Tel-Aviv 6779801, Israel
E-mail: mukeshsharma@mail.tau.ac.il
Dr. M. Sharma, Prof. T. Ellenbogen
Center for Light-Matter Interaction
Tel-Aviv University
Tel-Aviv 6779801, Israel
Dr. N. Hendler
The Chaoul Center for Nanoscale Systems
Tel-Aviv University
Tel-Aviv 6779801, Israel
The ORCID identification number(s) for the author(s) of this article can be found under https://doi.org/10.1002/adom.201901182.

DOI: 10.1002/adom.201901182

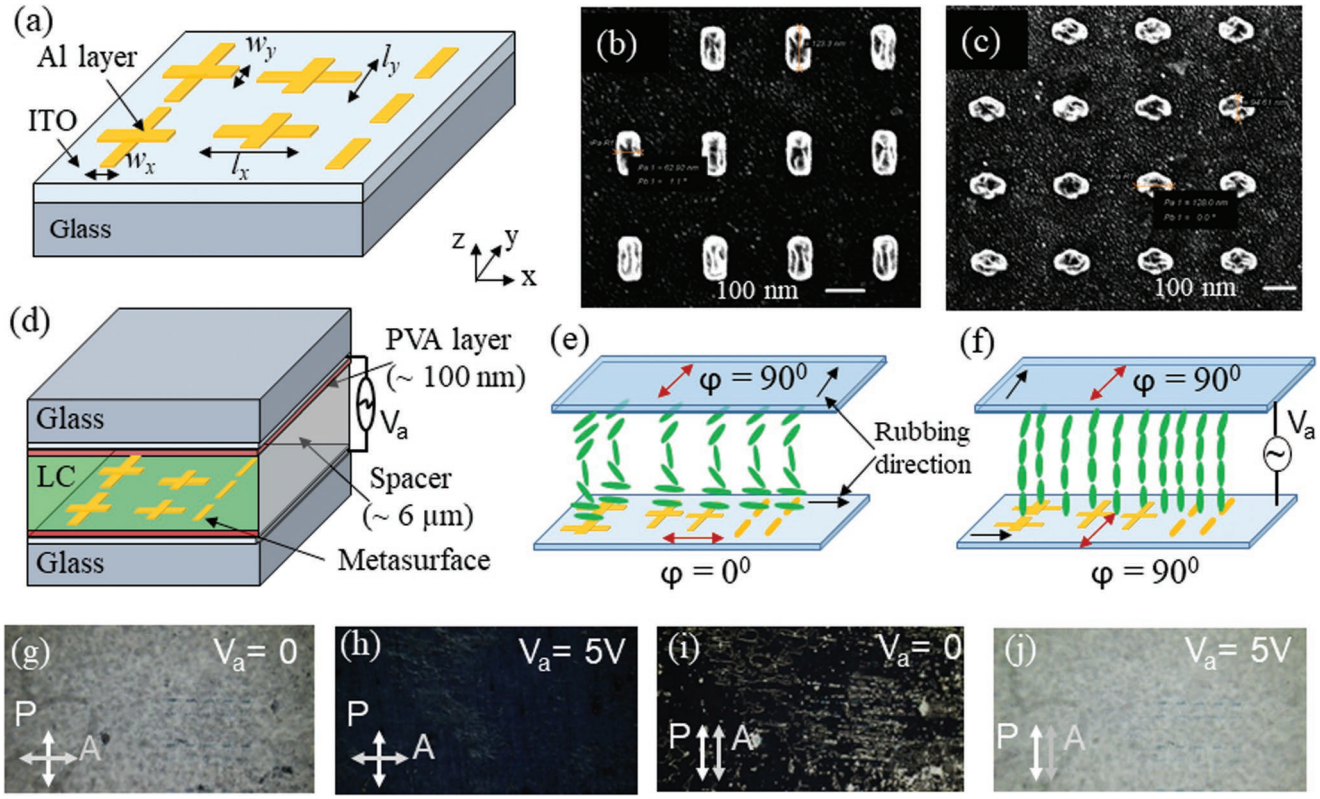

Figure 1. a) Schematic design of the proposed plasmonic metasurface and their nanostructures dimensions. b) SEM image of rod-shaped nanoantennas array and c) cross-shaped nanoantenna array. The scale bar is 100 nm for both SEM images. d) Schematic view of the integrated LC-plasmonic metasurface device. e) Schematic representation of the working principle of the TN-LC layer which rotates the polarization of incident *y*-polarized light ($\varphi = 90°$) by 90° and converts it to *x*-polarized light ($\varphi = 0°$) that excites the corresponding LSPR. f) The TN-LC layer changes its configuration when external voltage is applied and the incident polarization is maintained in the LC layer. Snapshots of the micrographic textures of the device under crossed-polarized condition of polarizer (P) and analyzer (A) at g) $V_a = 0$ and h) $V_a = 5$ V, and parallel-polarized condition of P and A at i) $V_a = 0$ and j) $V_a = 5$ V, respectively.

color filter. In both works, the color generation mechanism is based on the collective response of the array.

Here, we introduce and study an LC-chromatic plasmonic polarizers based platform for dynamic color manipulations. The color manipulation mechanism origins at the interaction between the LC and each of the single plasmonic nanoantennas. This allows to dynamically change the color of light transmitted, scattered, or reflected from each antenna at superior spatial resolution. Specifically, we use it to demonstrate electrically switchable plasmonic metasurface based color tags that may be interesting for security and display applications. To demonstrate the diversity of the color manipulation platform two different types of dynamic color tags are studied, which consist of color only sample based on rod-shaped nanoantennas (i.e., *NEO* pattern) and color contrast sample based on cross-shaped nanoantennas (i.e., *LC* pattern). These two types of configurations can be used for different applications such as active color pixels for color displays, security applications, and also as polarization detectors for polarization microscopy. The dynamic switching of transmitted colors, or interacting LSPR wavelength, is achieved by applying external voltage on the integrated LC-plasmonic metasurface layer. The developed devices have advantages in terms of their simple design, high potential spatial resolution, ease of fabrication, low threshold voltage operation and their electrically switchable transmission colors potentially spanning the entire visible spectrum. These experimental results of active integrated LC-plasmonic metasurface tags demonstrate new opportunities to realize the next generation of switchable or active multifunctional optical devices.

Figure 1a illustrates the schematic diagram of the proposed plasmonic metasurface. It consists of rod-shaped and cross-shaped nanoantenna arrays, fabricated on indium tin oxide (ITO) coated glass substrate, by using standard electron-beam lithography process (see the Experimental Section). The period of the nanoantenna arrays was 180 nm. The thicknesses of the ITO layer and the aluminum (Al) layer were 30 and 50 nm, respectively. The dimensions of each rod-shaped nanoantenna were l = 120 nm and w = 50 nm, where l and w are the length and width of the rod-shaped nanoantenna, respectively. Similarly, the dimensions of each cross-shaped nanoantennas were as follows: l_x = 120 nm, l_y = 80 nm, w_x = 50 nm, w_y = 50 nm, and their 90° rotation was l_x = 80 nm, l_y = 120 nm, w_x = 50 nm, and w_y = 50 nm, where subscripts *x* and *y* represent dimensions in *x* and *y* directions as illustrated in the figure. Scanning electron microscope (SEM) images of the metasurface having rod-shaped nanoantenna and cross-shaped nanoantenna arrays are shown in Figure 1b,c, respectively.

Figure 1d shows the schematic diagram of the integrated LC over the plasmonic metasurface. The top and bottom ITO-coated glass substrates work as the transparent electrodes of the device. A 100 nm thick layer of polyvinyl alcohol (PVA) was spin-coated over the top ITO-coated glass substrate and the bottom plasmonic metasurface layer, and gently rubbed with a velvet cloth to induce a prealignment of the LC molecules in a preferred direction. The rubbing directions on the two PVA-coated substrates were perpendicular to each other to promote the TN-LC configuration of the LC molecules. The device was assembled by using a 6 μm Mylar spacer between the PVA-coated substrates. In order to obtain efficient TN-LC configuration, the thickness of the spacer layer, which also determines the thickness of LC layer, should satisfy the Mauguin limit.[33–35] In our experiment, the nematic LC that was uses was 4-cyano-4′-pentylbiphenyl (5CB). The ordinary (n_o) and extraordinary (n_e) refractive indices of 5CB at room temperature and wavelength of 630 nm are $n_o = 1.53$ and $n_e = 1.71$, respectively. Figure 1e shows the initial TN-LC configuration, without applying external electric field, which converts the *y*-polarized ($\varphi = 90°$) incident light into *x*-polarized ($\varphi = 0°$) light. The initial TN-LC configuration can be changed by applying external electric field between the top and bottom electrodes. With application of the external electric field, the LC molecules start to reorient in the direction of applied electric field. At the saturation voltage ($V_a = 5$ V), after a certain response time, all LC molecules align in the same direction (perpendicular to the glass substrate) which eliminates the TN-LC configuration (Figure 1f). Therefore, in this situation, the *y*-polarized ($\varphi = 90°$) incident light passes through the LC layer without rotating the polarization direction at the interface of LC and plasmonic metasurface. Thus, the integrated TN-LC layer over the plasmonic metasurface is utilized to achieve active control of the polarization direction of the incident light that in turn modulates the polarization-dependent LSPR wavelength or transmission, reflection, and scattering colors of the nanoantenna arrays.

To confirm the TN-LC configuration after fabrication of the integrated LC-plasmonic metasurface, the device was placed under crossed and parallel polarizer and analyzer configurations and snapshots of micrographic textures have been taken at applied voltages $V_a = 0$ and $V_a = 5$ V (Figure 1g–j). From Figure 1g,h, it can be clearly seen that in the crossed-polarizer-analyzer condition, a bright surface is observed at $V_a = 0$, which shows that the polarization of the incident light is rotated by 90° through the TN-LC layer, and at $V_a = 5$ V, the elimination of the TN-LC configuration results in dark output. Similarly, the dark surface output is obtained in case of parallel polarizer-analyzer conditions at $V_a = 0$ (Figure 1i) and bright surface output is obtained at $V_a = 5$ V (Figure 1j). Under the crossed-polarizer-analyzer condition, the transmittance of the TN-LC layer drastically changed from 70% (with respect to glass sample without LC) to 3% when applied voltage changed from $V_a = 0$ (Figure 1g) to $V_a = 5$ V (Figure 1h), respectively. In the case of parallel polarizer and analyzer configuration, the transmittance of the TN-LC layer changed from 5% to 75% when applied voltage changed from $V_a = 0$ (Figure 1i) to $V_a = 5$ V (Figure 1j), respectively.

At first, the transmission spectra of the plasmonic metasurface based tags were studied before their integration in the TN-LC configuration. **Figure 2**a shows the SEM image of the fabricated *NEO* tag. Figure 2b,c indicates the transmission images of the nanorod based *NEO* tag without the LC layer when incident light was *x*-polarized ($\varphi = 0°$) and *y*-polarized ($\varphi = 90°$), respectively. The corresponding measured transmission spectra are shown in Figure 2d. It was observed that the *x*-polarized light ($\varphi = 0°$) excites LSPR at shorter wavelength of 476 nm, when it interacts with short axes ($w_x = 50$ nm) of the rod-shaped nanoantennas and as a consequence the *NEO* tag looks yellow in transmission, whereas the *y*-polarized light ($\varphi = 90°$), which is parallel to the long axes ($l_y = 120$ nm) of the nanoantennas array, excites LSPR at longer wavelength of 567 nm which corresponds to violate color in transmission (Figure 2b–d). The real-time experimental demonstration is shown in Movie S1 (Supporting Information) which demonstrates the variation in transmitted colors of the tag due to mechanically rotating the input polarizer from $\varphi = 90°$ to $\varphi = 0°$. Figure 2e–o presents the experimental transmission images and spectra of the *NEO* tag after integration with LC layer. One can see from the measured transmission spectra that two significant effects are observed. First, the LSPR wavelengths are redshifted (see Figure 2d and l,m), in comparison to *NEO* tag without LC layer, for both polarizations of lights $\varphi = 0°$ (525 nm) and $\varphi = 90°$ (627 nm), with a maximum wavelength shift of ≈60 nm. This is primarily due to the increasing refractive index of the surrounding dielectric medium of the nanoantennas from air (refractive index, $n_{air} = 1$) to the PVA layer (≈100 nm) (refractive index, $n_{PVA} \approx 1.5$). The resonance redshift is due to the reduction of surface plasmon wavelength by the higher index of the surrounding PVA layer.[36] Second, at applied voltage $V_a = 0$, the incident light is rotated by 90° when it passes through the TN-LC layer. When the incident light is *x*-polarized, after passing through the TN-LC layer, it is converted into a *y*-polarized light, and finally, it interacts with the metasurface and excites the *y*-polarized LSPR wavelength and vice versa. It can be seen that the excited LSPR wavelengths are 626 and 526 nm for $\varphi = 0°$ and $\varphi = 90°$, respectively, at $V_a = 0$ (see Figure 2l).

When external voltage is applied to the electrodes, the LC molecules start to reorient in the direction of field. As the applied voltage increases beyond a threshold voltage[16] $V_a = 1$ V, the TN-LC changes its configuration (see Figure 1f), and as a result the transmitted light maintains its original polarization. This effect provides the key to obtain electrical switching of the interaction of light with specific LSPR and as a consequence to obtain change in the transmission and reflection colors of the fabricated LC-plasmonic metasurface device. Figure 2f,i shows the transmission photographs of the *NEO* tag for $\varphi = 0°$ and $\varphi = 90°$, respectively, at $V_a = 2$ V. Figure 2g,j shows the transmission photographs of the *NEO* tag for $\varphi = 0°$ and $\varphi = 90°$, respectively, at $V_a = 5$ V, and Figure 2l shows the corresponding transmission spectra. It can be seen that with external voltage of 5 V the interaction with the LSPR is switched with respect to the case of 0 V (Figure 2e,h,l). Figure 2k shows the calculated color modulation segment on the CIE 1931 *xy* chromaticity diagram with applied voltage for the *x*-polarized incident light ($\varphi = 0°$).

We also studied the gradual variation of the interaction with the two LSPR wavelengths or transmission colors of the *NEO* tag with varying applied voltages from $V_a = 0$ to

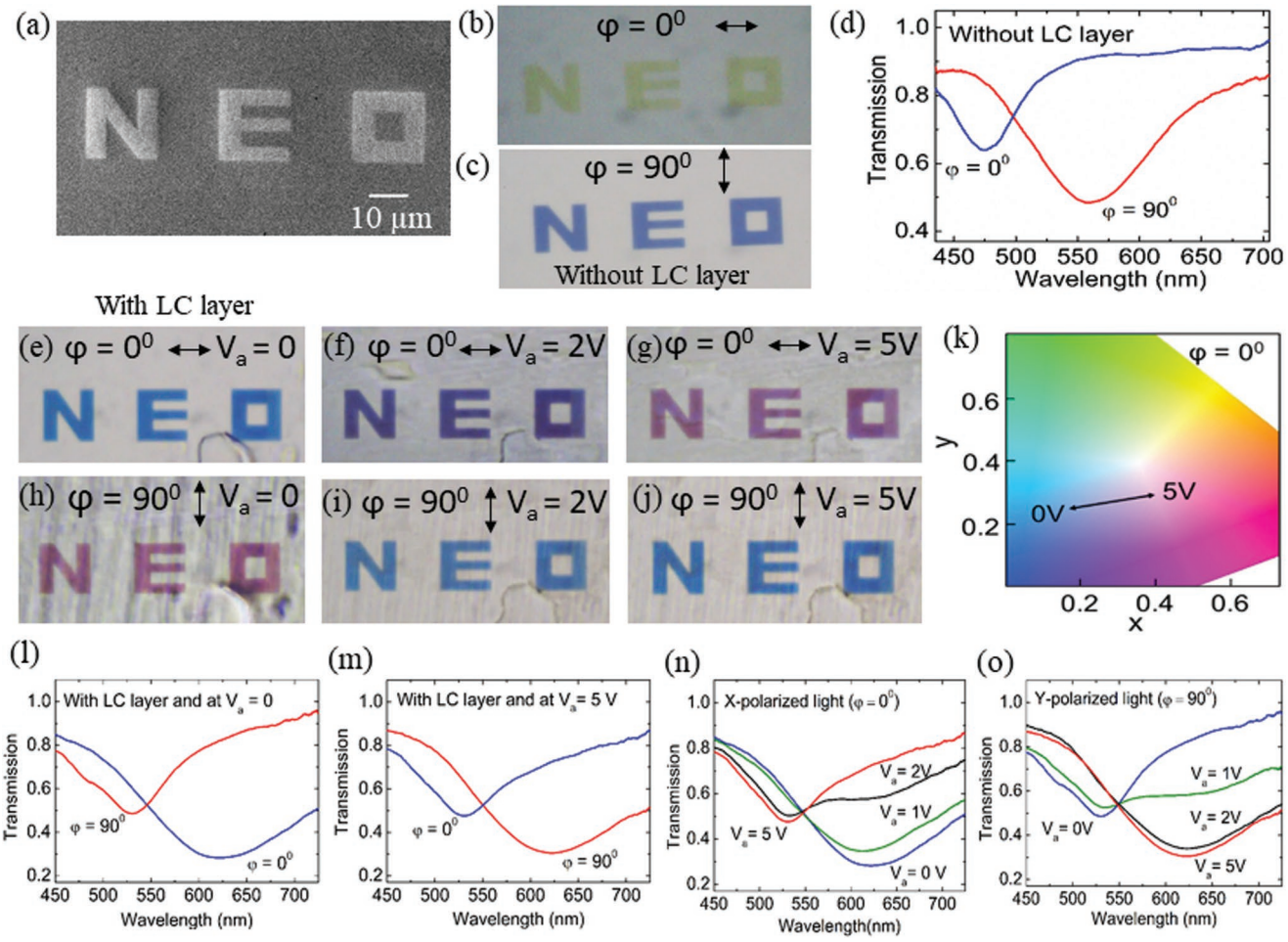

Figure 2. Demonstration of the fabricated *NEO* tag. a) SEM image of rod-shaped nanoantennas array based *NEO* tag. The scale bar is 10 μm long. b,c) Transmission images of *NEO* tag, without LC layer for *x*-polarized incident light ($\varphi = 0°$) and for *y*-polarized incident light ($\varphi = 90°$). d) Measured transmission spectrum of plasmonic metasurface before integrating the LC layer for polarization angles of $\varphi = 0°$ and $\varphi = 90°$. e–g) Transmission image of *NEO* tag, with LC layer for $\varphi = 0°$ at $V_a = 0$, $V_a = 2$ V, and $V_a = 5$ V. h–j) Transmission images for $\varphi = 90°$ at $V_a = 0$, $V_a = 2$ V, and $V_a = 5$ V. k) Mapping of calculated color modulation segment on the CIE 1931 *xy* chromaticity diagram with applied voltage for the *x*-polarized incident light ($\varphi = 0°$). l,m) Transmission spectra for linearly *x*-polarized light ($\varphi = 0°$) and *y*-polarized light ($\varphi = 90°$) at $V_a = 0$ and $V_a = 5$ V. n) Transmission spectra of *NEO* tag with LC layer at various applied voltages $V_a = 0$, 1, 2, and 5 V under the *x*-polarized incident light ($\varphi = 0°$) condition. The interacting LSPR wavelength electrically tuned from 626 to 525 nm when the applied voltage changes from $V_a = 0$ to $V_a = 5$ V. o) Transmission spectra of *NEO* tag with LC layer at various applied voltages $V_a = 0$, 1, 2, and 5 V when incident light is *y*-polarized ($\varphi = 90°$).

$V_a = 5$ V (see Figure 2n,o). In this experiment, the incident polarization was fixed and only the applied voltage was changed from $V_a = 0$ to 5 V in steps of 0.5 V. One can see that the LSPR wavelength in the transmission spectrum is electrically tuned from 626 nm (at $V_a = 0$) to 525 nm (at $V_a = 5$ V) when incident light is *x*-polarized ($\varphi = 0°$) (see Figure 2e–g and n). The real-time experimental demonstration is shown in Movie S2 (Supporting Information). In case of *y*-polarized ($\varphi = 90°$) light, the LSPR wavelength is tuned from 526 nm (at $V_a = 0$) to 627 nm (at $V_a = 5$ V), with a maximum tuning shift of ≈101 nm (see Figure 2h–j and o). Correspondingly, the transmission colors of the tag are changed between blue and orange. These experimental results indicate that the fabricated LC-plasmonic metasurface platform allows to actively and efficiently control the interaction with specific LSPR wavelengths and the transmission colors, even at very low applied voltage.

Next, we also experimentally demonstrate the LC-based active control mechanism on metasurface-based tag (namely, *LC*) constructed from chromatic plasmonic polarizers[2] (see Figure 1a,c) where the nanoantennas that form the letters and those that form the background are rotated by 90°. This type of configuration can be used to obtain large color contrast of the tag for various applications.[2] Two polarization-dependent LSPR wavelengths of 509 and 566 nm for $\varphi = 0°$ and $\varphi = 90°$, respectively, were observed in the transmission spectrum measurements (**Figure 3**a,b,i) of the plasmonic metasurface tag (without LC layer). It can be seen that the background and the inside area of the letter (see Movie S3, Supporting Information) have generated the inversely separate transmission colors for incident *x*-polarized light ($\varphi = 0°$) (yellow and blue color) and *y*-polarized light ($\varphi = 90°$) (blue and yellow color), respectively. This strong color contrast occurs due to the 90° rotation of the cross-shaped

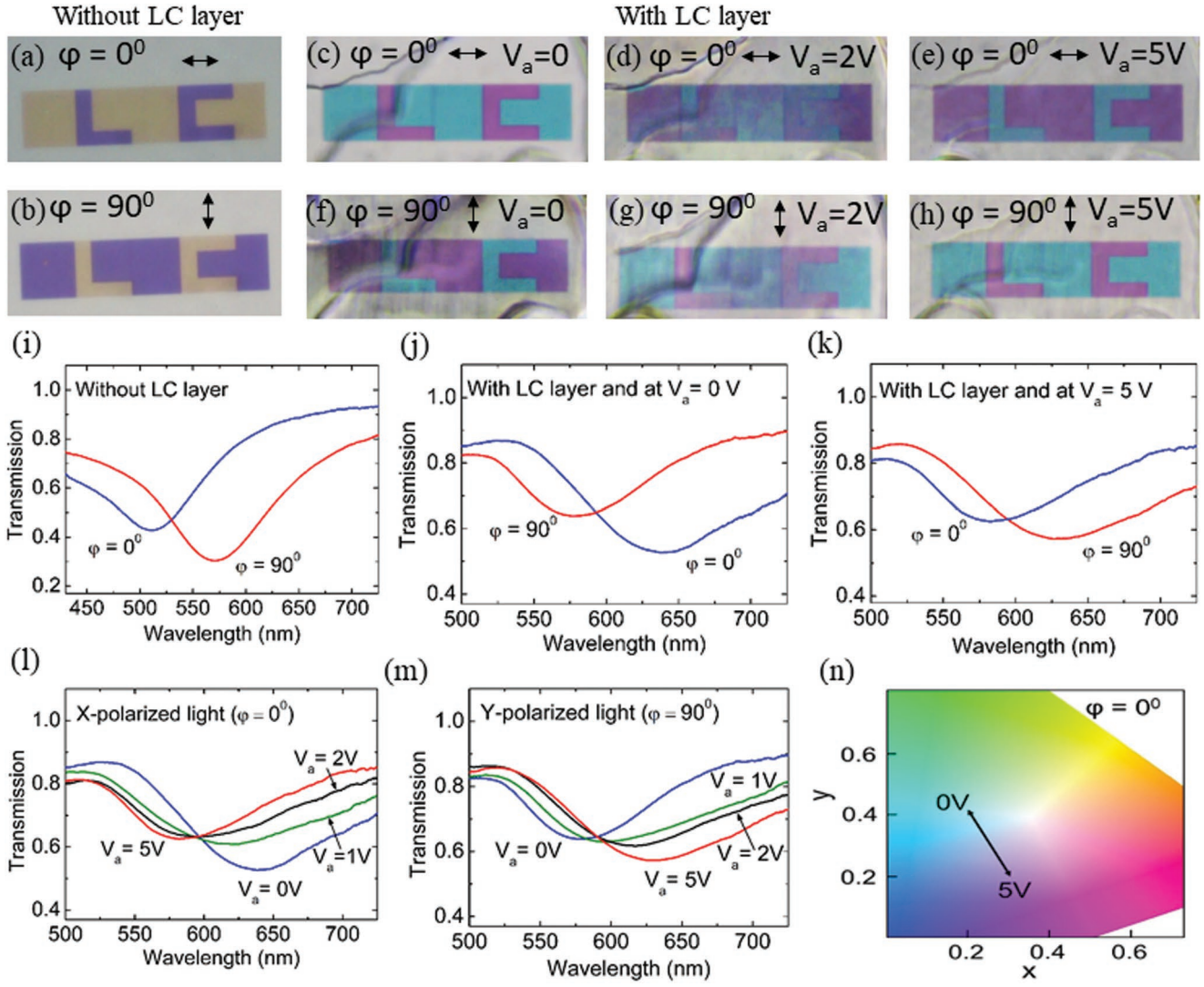

Figure 3. Demonstration of the fabricated *LC* tag. a,b) Transmission images of *LC* tag without LC layer for $\varphi = 0°$ and $\varphi = 90°$. Transmission images of *LC* tag after integrating with LC layer for c) $\varphi = 0°$ at $V_a = 0$, d) at $V_a = 2$ V, and e) at $V_a = 5$ V, f) for $\varphi = 90°$ at $V_a = 0$, g) at $V_a = 2$ V, and h) at $V_a = 5$ V. i–k) Measured transmission spectra for polarization angles of $\varphi = 0°$ and $\varphi = 90°$, before integrating LC layer, with LC layer at $V_a = 0$, and with LC layer at $V_a = 5$ V. l) Transmission spectra of *LC* tag with LC layer at various applied voltages $V_a = 0$, 1, 2, and 5 V under the *x*-polarized incident light ($\varphi = 0°$) condition. The LSPR wavelength is electrically tuned from 632 to 587 nm when the applied voltage changes from $V_a = 0$ to $V_a = 5$ V. m) Transmission spectra of *LC* tag with LC layer at various applied voltages $V_a = 0$, 1, 2, and 5 V when incident light is *y*-polarized ($\varphi = 90°$). The LSPR wavelength shifts from 584 to 630 nm when the applied voltage changes from $V_a = 0$ to $V_a = 5$ V. n) Mapping of calculated color modulation segment on the CIE 1931 *xy* chromaticity diagram with applied voltage for the *x*-polarized incident light ($\varphi = 0°$).

nanoantennas array in the letter with respect to the background. After the coating of the metasurface with the alignment PVA layer, the LSPR wavelengths were redshifted, as expected. In addition, due to the rotation of polarization of incident light by 90° through TN-LC configuration, the corresponding color change was also observed on *LC* tag at $V_a = 0$ (Figure 3i,j). It was found that the same transmission colors were generated by *LC* tag with LC layer for $\varphi = 0°$ at $V_a = 0$ (Figure 3c) and $\varphi = 90°$ at $V_a = 5$ V (Figure 3h). Simultaneously, the same transmission colors appeared for $\varphi = 90°$ at $V_a = 0$ (Figure 3f) and for $\varphi = 0°$ at $V_a = 5$ V (Figure 3e), respectively. The corresponding LSPR wavelengths were measured in the transmission spectra of the background of the tag, as presented in Figure 3i–k.

For further experimental analysis, we measured the electro-optic characteristics of the *LC* tag, for fixed input polarized light, by varying the applied voltage from $V_a = 0$ to $V_a = 5$ V. Figure 3l,m depicts the variation of the LSPR wavelengths with varying applied voltage in both conditions of incident *x*-polarized ($\varphi = 0°$) and *y*-polarized ($\varphi = 90°$) light, respectively. The interacting LSPR wavelength, for incident polarization $\varphi = 0°$, is electrically tuned from 632 to 587 nm when applied voltage varying from $V_a = 0$ to $V_a = 5$ V, respectively (see Movie S4, Supporting Information). In the case of $\varphi = 90°$, it shifts from 584 to 630 nm with applied voltages changing from $V_a = 0$ to $V_a = 5$ V, respectively. The color modulation segment on the CIE 1931 *xy* chromaticity diagram for *LC* tag with applied voltage

for the *x*-polarized incident light ($\varphi = 0°$) is shown in Figure 3n, which also demonstrates the voltage-dependent color modulation of the *LC* tag.

In conclusion, our study demonstrates electrically controlled dynamic color-tuning tags based on active LC-plasmonic metasurface platform exploiting a TN-LC configuration as a polarization rotator. We show that this configuration allows to control the interaction of light with the different plasmonic resonances of the metasurface. As a consequence, the transmitted colors and spectra of these devices can be gradually modified or changed abruptly by controlling the applied voltage. Such active LC-plasmonic metasurface based platform can be used to construct a variety of high-efficiency dynamic devices to control color or spectra, which are developed at a low cost, with easy fabrication process, work at low driving voltages, and have compact size. These attractive features may be of great interest for future development of switchable or multifunctional devices at nanoscale.

Experimental Section

Fabrication of Plasmonic Metasurface Tags: An ITO-coated glass substrate (30 nm thick ITO layer, Sigma-Aldrich) was cleaned and then spin-coated with a positive e-beam resist poly(methyl methacrylate) (PMMA), followed by baking at 180 °C on a hot plate for 2 min. The nanostructure arrays of rod-shaped and cross-shaped nanoantennas with patterns ("LC" and "NEO") were written by an electron-beam lithography system (Raith 150 II) at an accelerating voltage of 10 kV and followed by developing the patterns. A 50 nm thin layer of aluminum was deposited by using the E-gun evaporator. Lift-off process was carried out by using acetone.

Fabrication of Active LC-Plasmonic Metasurface Device: The bottom substrate with the nanostructured tags was spin-coated with a planar alignment layer of PVA (≈100 nm thickness), followed by baking at 120 °C for 30 min and subsequent cooling to room temperature. The baked PVA layer was then rubbed mechanically in the *x*-direction by using a soft velvet cloth. The same procedure was followed on the ITO-coated glass top substrate. This substrate was spin-coated with PVA layer and treated with mechanical rubbing along the *y*-direction. The rubbing directions on these two substrates were orthogonal to each other to promote a TN-LC conformation of LC molecules. The substrates were assembled together with a Mylar spacer layer of 6 µm (Sigma-Aldrich) by using UV-curable adhesive NOA61 followed by UV curing. After this stage, the electrical contacts were made on the top and bottom substrates using a thin aluminum wire and silver conducting paint. The nematic LC 5CB was infiltrated into the empty LC-plasmonic metasurface (with gap of 6 µm), with the help of a thin needle, by capillary action. During the LC infiltration procedure, the fabricated device was kept on a hot plate which maintained temperature at 50 °C. At this temperature, the nematic LC 5CB is in its isotropic phase, which has lower viscosity than its nematic phase and therefore it can be easily infiltrated into the gap.

Spectral Characterization of Active LC-Plasmonic Metasurface Device: The transmission spectra of the fabricated LC-plasmonic metasurface device were measured using an imaging spectrometer (Andor, Shamrock 303i), which was optically connected to the output of an optical microscope (Zeiss axio observer Z1m), using an optical relay. During the experiment, incident white light was first passed through a polarizer to convert into linear polarization and then was incident normal onto the LC-plasmonic metasurface. The transmission spectra of the tags were recorded for both *x*-polarized ($\varphi = 0°$) and *y*-polarized ($\varphi = 90°$) light in the cases of with and without the LC layer. All the recorded data were normalized with respect to the bare ITO-coated glass substrate the area where there were no tags. Optical microscopy images of the illuminated tags area were captured by a Canon color camera that was attached to the optical microscope. In our experiments, it is important to note that the incident polarized light first travels through the LC layer and then interacts with the plasmonic metasurface. For electro-optic characterization, the LC-plasmonic metasurface device was connected to a function generator to provide an alternating current (AC) square signal wave of frequency 1 kHz to modulate the optical properties of the LC molecules.

Supporting Information

Supporting Information is available from the Wiley Online Library or from the author.

Acknowledgements

This research was supported by the Israeli Ministry of Science Grant Agreement No. 81604. The authors would like to thank Ori Avayu and Dr. Stanislav Stepanov for help during the fabrication process of plasmonic metasurface prototypes. M.S. acknowledges the support from the Israeli Ministry of Science for the Postdoc Fellowship.

Conflict of Interest

The authors declare no conflict of interest.

Keywords

liquid crystals, localized surface plasmons, plasmonic metasurfaces, tunable color devices

Received: July 14, 2019
Revised: November 20, 2019
Published online: January 20, 2020

[1] N. I. Zheludev, Y. S. Kivshar, *Nat. Mater.* **2012**, *11*, 917.
[2] T. Ellenbogen, K. Seo, K. B. Crozier, *Nano Lett.* **2012**, *12*, 1026.
[3] X. Duan, S. Kamin, N. Liu, *Nat. Commun.* **2017**, *8*, 14606.
[4] A. Nemati, Q. Wang, M. Hong, J. Teng, *Opto-Electronic Adv.* **2018**, *1*, 180009.
[5] T. Li, L. Huang, J. Liu, Y. Wang, T. Zentgraf, *Opt. Express* **2017**, *25*, 4216.
[6] N. Jiang, X. Zhuo, J. Wang, *Chem. Rev.* **2018**, *118*, 3054.
[7] L. Kang, R. P. Jenkins, D. H. Werner, *Adv. Opt. Mater.* **2019**, *7*, 1801813.
[8] A. M. Shaltout, V. M. Shalaev, M. L. Brongersma, *Science* **2019**, *364*, 648.
[9] O. Buchnev, N. Podoliak, M. Kaczmarek, N. I. Zheludev, V. A. Fedotov, *Adv. Opt. Mater.* **2015**, *3*, 674.
[10] K. Xiong, D. Tordera, M. P. Jonsson, A. B. Dahlin, *Rep. Prog. Phys.* **2019**, *82*, 024501.
[11] W. L. Barnes, A. Dereux, T. W. Ebbesen, *Nature* **2003**, *424*, 824.
[12] O. Avayu, E. Almeida, Y. Prior, T. Ellenbogen, *Nat. Commun.* **2017**, *8*, 14992.
[13] J. Rensberg, S. Zhang, Y. Zhou, A. S. McLeod, C. Schwarz, M. Goldflam, M. Liu, J. Kerbusch, R. Nawrodt, S. Ramanathan, D. N. Basov, F. Capasso, C. Ronning, M. A. Kats, *Nano Lett.* **2016**, *16*, 1050.

[14] T. Cui, B. Bai, H. B. Sun, *Adv. Funct. Mater.* **2019**, *29*, 1806692.
[15] K. Kumar, H. Duan, R. S. Hegde, S. C. W. Koh, J. N. Wei, J. K. W. Yang, *Nat. Nanotechnol.* **2012**, *7*, 557.
[16] D. K. Yang, S. T. Wu, *Fundamentals of Liquid Crystal Devices*, Wiley, Hoboken, NJ **2006**.
[17] I. C. Khoo, *Liquid Crystals*, Wiley, Hoboken, NJ **2007**.
[18] S. Homaeigohar, M. Elbahri, *Adv. Opt. Mater.* **2019**, *7*, 1801101.
[19] M. L. Tseng, J. Yang, M. Semmlinger, C. Zhang, P. Nordlander, N. J. Halas, *Nano Lett.* **2017**, *17*, 6034.
[20] M. Kim, I. Kim, J. Jang, D. Lee, K. T. Nam, J. Rho, *Appl. Sci.* **2018**, *8*, 982.
[21] Q. Wang, E. T. F. Rogers, B. Gholipour, C. M. Wang, G. Yuan, J. Teng, N. I. Zheludev, *Nat. Photonics* **2016**, *10*, 60.
[22] J. Olson, A. Manjavacas, T. Basu, D. Huang, A. E. Schlather, B. Zheng, N. J. Halas, P. Nordlander, S. Link, *ACS Nano* **2016**, *10*, 1108.
[23] M. Decker, C. Kremers, A. Minovich, I. Staude, A. E. Miroshnichenko, D. Chigrin, D. N. Neshev, C. Jagadish, Y. S. Kivshar, *Opt. Express* **2013**, *21*, 8879.
[24] Z. Ma, X. Meng, X. Liu, G. Si, Y. J. Liu, *Nanomaterials* **2018**, *8*, 871.
[25] G. Si, Y. Zhao, E. S. P. Leong, Y. J. Liu, *Materials* **2014**, *7*, 1296.
[26] Y. C. Hsiao, C. W. Su, Z. H. Yang, Y. I. Cheypesh, J. H. Yang, V. Y. Reshetnyak, K. P. Chen, W. Lee, *RSC Adv.* **2016**, *6*, 84500.
[27] Y. Lee, M. K. Park, S. Kim, J. H. Shin, C. Moon, J. Y. Hwang, J. C. Choi, H. Park, H. R. Kim, J. E. Jang, *ACS Photonics* **2017**, *4*, 1954.
[28] Y. Zhang, Q. Liu, H. Mundoor, Y. Yuan, I. I. Smalyukh, *ACS Nano* **2015**, *9*, 3097.
[29] H. Su, H. Wang, H. Zhao, T. Xue, J. Zhang, *Sci. Rep.* **2017**, *7*, 17378.
[30] W. Dickson, G. A. Wurtz, P. R. Evans, R. J. Pollard, A. V. Zayats, *Nano Lett.* **2008**, *8*, 281.
[31] A. Komar, R. P. Domínguez, A. Miroshnichenko, Y. F. Yu, Y. S. Kivshar, A. I. Kuznetsov, D. Neshev, *ACS Photonics* **2018**, *5*, 1742.
[32] S.-Q. Li, X. Xu, R. M. Veetil, V. Valuckas, R. P. Domínguez, A. I. Kuznetsov, *Science* **2019**, *364*, 1087.
[33] M. Schadt, W. Helfrich, *Appl. Phys. Lett.* **1971**, *18*, 127.
[34] Z. Zhuang, Y. J. Kim, J. S. Patel, *Appl. Phys. Lett.* **2000**, *76*, 3995.
[35] T. X. Wu, Y. Huang, S.-T. Wu, *Jpn. J. Appl. Phys.* **2003**, *42*, L39.
[36] L. Novotny, *Phys. Rev. Lett.* **2007**, *98*, 266802.

